Journal of Alloys and Compounds 1030 (2025) 180786

Contents lists available at ScienceDirect

Journal of Alloys and Compounds

journal homepage: www.elsevier.com/locate/jalcom

Development of low-cost Ti alloys with a balanced strength and ductility with generation of ultra-fine microstructures

Zhiyi Zou [a], Matthew K. Dunstan [b], Brandon McWilliams [b], Stuart Robertson [c], Richard Hague [a], Marco Simonelli [a,*]

[a] Centre for Additive Manufacturing, University of Nottingham, Nottingham NG8 1BB, UK
[b] DEVCOM Army Research Laboratory, Aberdeen Proving Ground, Aberdeen, MD 21005, USA
[c] Department of Materials, Loughborough Materials Characterisation Centre, Loughborough University, Loughborough, Leicestershire LE11 3TU, UK

ARTICLE INFO

Keywords:
Titanium alloys
Ultrafine grained microstructure
Deformation structure
Ductility
Ti-Cr-Sn alloy

ABSTRACT

This study aims to understand the interplay between strength and ductility in metastable β-Ti alloys based on eutectoid and neutral elements. A low-cost ternary Ti-7Cr-4Sn alloy was prepared by furnace cooling from the single β region at the end of the primary processing. Although isothermal ω, a nano-precipitation generally considered to embrittle the material, is present in the obtained ultra-fine microstructure, the material still exhibits a balanced strength and ductility, with a yield stress of 1067 MPa and elongation of about 10 %. The obtained tensile properties surpass traditional primary processed Ti-6Al-4V, and are comparable to a range of expensive commercial high-strength aerospace Ti alloys. Multiple microstructural features, including grain boundary α (α_{GB}), short rod shape primary α (α_P), isothermal ω (ω_{iso}) and ω assisted secondary α (α_s) are characterised within the room temperature microstructure. Microstructural analysis reveals that strong Cr segregation in the β phase and slight partitioning of Sn between the α and β phase strengthens the β phase while also preserving ductility in the alloy. This results in a microstructure dominated by the ductile α phase and submicron α grain boundaries. This study also discusses the evolution of these microstructural features during different stages of cooling from β matrix, substantiating a promising alloy design strategy for affordable high-performance new Ti alloys.

1. Introduction

Thanks to their high specific strength, Titanium (Ti) alloys are generally considered the most promising structural materials for lightweight applications [1]. However, the high cost of Ti alloys limits their use in many engineering applications [2]. Apart from the cost of raw materials, the production cost notably contributes to the overall price of the Ti alloys [3,4].

During Ti alloy production, multiple heat treatments and thermomechanical processes, also known as downstream processing, are commonly applied after primary processing to balance the material's strength and ductility, as a good combination of such two properties is crucial for performance [1,5]. These additional processes are known to significantly increase the production cost of Ti alloys and may account for roughly 20–50 % of the total production costs [4,6]. Therefore, it is of great interest to develop Ti alloys with relatively cheap constitutions while requiring minimum downstream processing.

Near/metastable β-Ti alloys may offer the potential to deliver a good balance of strength and ductility without the need for hot working, as evidenced by multiple novel Ti alloys developed in the past 5 years [7–10], and thus reduce the overall production costs. The decomposition of the metastable β-Ti and other intermediate phases (ω, o, o', etc.) can lead to the formation of a broad range of microstructures [11], providing, in turn, the ability to tailor the resulting mechanical properties. Such intermediate phases assisted phase transformation pathways have been recently reviewed in detail by Gupta, Khatirkar and Singh [5], as well as by Liu, Li, Gu and Song [12]. Furthermore, microstructure engineering that utilises such pathways can develop Ti alloys with hierarchical microstructure to achieve strong and ductile performance [8,9,13–15].

For example, research suggests that upon slow cooling from above the β transus temperature, isothermal ω phase (ω_{iso}) might form [14,16], and the presence of ω_{iso} then might assist the formation of refined dual phase α+ β microstructures [14,17]. Latest Transmission Electron

* Corresponding author.
E-mail address: Marco.Simonelli@nottingham.ac.uk (M. Simonelli).

https://doi.org/10.1016/j.jallcom.2025.180786
Received 5 February 2025; Received in revised form 29 April 2025; Accepted 4 May 2025
Available online 5 May 2025

Microscopy (TEM) observations [14,18] revealed that, as a solution-lean nanoscale precipitate homogeneously distributed in the β matrix, ω_{iso} phase introduces uniformities at both compositional and structural levels [19,20]. Therefore, the ω_{iso}/β interface is thought to act as the preferred nucleation site for the α phase within the β matrix [20,21]. Such a ω-assisted α nucleation has been identified and detail characterised in multiple metastable β-Ti alloys [12,18,22]. Competitive growth between α and β would then lead to a refined dual-phase grain structure [14,15,20]. Such fine microstructures have recently attracted considerable interest as they inherently promote material strengths [1, 15,23,24]. However, the ductility associated with these microstructures is somewhat uncertain: some studies report noticeable embrittlement following the formation of α+ β microstructures via the ω phase [11,17, 24–26], while other works report good or even enhanced ductility with respect to alloys made of single (precursor) metastable β phase [17, 26–29], leaving questions on the applicability of these alloys. In some cases, significant differences in the material's strength and ductility are imposed only by slight variations in temperature or time of the ω-related ageing [26,29].

Leveraging such ω-assisted α-refinement, this study aims to shed light on the strength and ductility interplay in a low-cost novel ternary Ti-Cr-Sn alloy. The Ti-Cr-Sn ternaries have shown interesting mechanical properties [30–32] and offer a viable low-cost composition. Recent research also demonstrated that Ti-Cr-Sn alloys are likely bio-compatible and have potential for biomedical applications [30,33].

As of today, most commercially available metastable Ti alloys are heavily formulated with expensive isomorphous β stabilisers, which increase raw material costs [1,34,35]. Latest research suggests that adapting eutectoid β stabilisers (e.g. Cr, Fe, Cu) in the material formulation to minimise the usage of isomorphous β stabilisers is a convincing approach to developing low-cost metastable Ti alloys [7,8,10]. For the Ti-Cr-Sn ternaries focused on in this study, the commonly used expensive isomorphous β stabilisers, such as V and Mo, are replaced by eutectoid β stabiliser, Cr, and a neutral element, Sn, effectively reducing the raw material cost. Based on the London Metal Exchange and Shanghai Metals Market, on September 2024, for 99 % purity metal, the average market price for Cr is 8 USD/kg, Sn is 30 USD/kg, while V is 160 USD/kg and Mo is 60 USD/kg [36,37].

In addition, since eutectoid β stabilisers have a high tendency to introduce ω precipitation [20], it is thought that using eutectoid β element as the only β stabiliser could also maximise the ω_{iso} formation, and in turn, more pronounced ω-assisted α nucleation. Likewise, moderate concentrations of Sn (<5 wt%) in eutectoid systems are thought to enhance strength by solution strengthening, and promote the formation of α phase during cooling [38,39], though the influence of Sn on ductility remains unclear.

In this context, this study intends to understand how the refined dual-phase microstructures develop in ternaries based on eutectoid β stabilisers (i.e. Cr) and so-called neutral elements (i.e. Sn), and discuss how the microstructural features affect the strength and ductility of these materials. A further understanding of the strength and ductility interplay in such refined microstructures would provide insights into future microstructure engineering and alloy design.

2. Methodology

2.1. Material used in this study

As determined in previous related investigations [40], Cr and Sn concentrations of approximately 7 and 4 wt%, respectively, allow for good castability without cracks, whilst promoting the formation of a metastable β phase. Moreover, a higher amount of Cr addition tends to stabilise the β phase and promote the possibility of β fleck formation, while a higher amount of Sn addition tends to suppress the precipitation of the ω phase [30,32,33,40]. Meanwhile, a lower amount of alloy elements will compromise the alloying strengthening of the material. We therefore used this composition as a model alloy for this study.

The designed material was achieved by melting industrially pure Ti/Cr sponges (Jiangxi Hongke Special Alloys LLC, China) and Sn billets (XI'AN Function Material Group CO., LTD, China) in a vacuumed electric arc furnace. The production route following melting is schematically illustrated in Fig. 1. The material was first hot-pressed at a temperature well above the β transus (950°C to 900°C), to produce a Φ65 mm ingot. Slow furnace cooling in the argon atmosphere was then applied to maximise any ω-assisted α nucleation, and allow newly formed α to grow to the preferred grain size. The furnace cooling lasted for roughly 15 hours, equivalent to an average cooling rate of ~1 °C/min. It should be noted that the real-time cooling rate varied at different furnace temperatures, with the cooling rate higher at a higher temperature. Once it reached room temperature, a 2.5 mm thick outer layer was removed to clear away any oxidised surface and produce Φ60 mm bars used for this study. It can be noted that minimal heating and thermo-mechanical processes are involved in the material production. The bars are only subjected to primary processing without additional downstream processing.

The exact composition of the bars was then determined via the inductively coupled plasma-optical emission spectrometry (ICP-OES), and is reported in Table 1 (for the sake of clarity, this composition is abbreviated as Ti-7Cr-4Sn hereafter). The corresponding β transus temperature, directly calculated from specimens taken from the bars, is 810 ± 10 °C, as ascertained by Simultaneous Differential Analysis (SDT).

2.2. Tensile tests and microstructural characterisation

To test the tensile properties of this alloy, three flat tensile specimens with a thickness of 1.5 mm and gauge length of 25 mm were machined from the bars according to standard ASTM E8/E8M-16a [41]. Room temperature tensile tests were conducted on an Instron 5969 with a video gauge at a strain rate of 0.15 mm/min.

Prior to microstructure characterisation, the samples were mirror-polished following the guidelines stated elsewhere [40]. A final chemical-mechanical polishing with a mixture of 0.03 μm colloidal silica suspension (OP-S) and hydrogen peroxide (H2O2, 30 % diluted) on an MD-chem cloth (Struers) was applied to prepare samples ready for microscopy analysis. Where needed, microstructure features were revealed by etching with Kroll's reagent.

The typical microstructural features were observed using a JEOL 6060LV SEM via secondary electron imaging. The crystallographic texture was investigated via Electron Back-Scattered Diffraction mapping (EBSD) and Transmission Kikuchi Diffraction mapping (TKD)

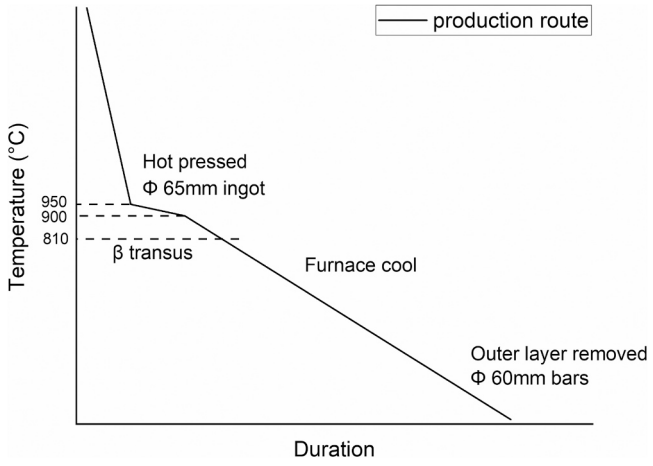

Fig. 1. The schematic temperature profile illustrates the production route for the Ti-7Cr-4Sn bars used for this study.

Table 1
The composition of the Ti-Cr-Sn alloy investigated in this study determined by ICP-OES.

	Ti	*Cr*	*Sn*	*O*	*C*	*H*	*N*	*Fe*
wt%	*Bal.*	*7.21 ± 0.25*	*3.93 ± 0.12*	*0.13 ± 0.02*	*< 0.01*	*< 0.01*	*0.08*	*< 0.1*

through a Helios G4 Xe PFIB DualBeam. EBSD maps are scanned using 13 nA current, 15 kV beam energy and a step size of 100 nm. TKD maps are scanned using 6.7 nA current, 30 kV beam energy and a step size of 20 nm. The collected data was analysed using AztecCrystal. Where needed, Scanning Transmission Electron Microscopy (STEM) analysis was conducted using a Tecnai F20 FEG-STEM. Additionally, synchrotron X-ray diffraction analysis was conducted at the I12 beamline in the Diamond Light Source UK, where a monochromatic beam of 100.096 keV (wavelength of $\lambda = 0.12386$ Å) and an exposure time of 2 s was used to determine the phases present in the material before and after tensile testing.

3. Results

3.1. Microstructure of the obtained material prior to tensile testing

The typical microstructure of the obtained flat specimens is shown in Fig. 2. Notable β flecks are not observed in the obtained billet (Fig. 2(a)), as expected in the material design. The observed material consists of quasi-equiaxed prior-β grains with an average equivalent diameter of approximately 300 μm (Fig. 2(a)), as measured via the line intercept method on multiple micrographs. Fig. 2(b) suggests that prior-β grains are composed of ultra-fine α+ β lamella arranged in a basketweave morphology, while continuous grain boundary α (α_{GB}) can be observed at the prior-β grain boundary, as pointed out by white arrows in Fig. 2 (b). The α_{GB} appears thicker than the α lath, but still has a relatively fine thickness of less than 1 μm. The typical crystallographic texture of the basketweave dual phase pattern is shown in Fig. 2(c) and (d). Statistics from the EBSD maps suggest that the alloy consists of approx. 66 % α phase and 34 % β phase, while the α lath has an average thickness of 0.47 ± 0.25 μm, and the β lath has an average thickness of 0.54 ± 0.34 μm. It is noteworthy that the α and β laths have similar thicknesses and are well within the sub-micron range. Since the EBSD maps here report a sufficiently large dataset in a homogeneous material, with over 6000 α/β laths identified in a randomly selected approx. 75 μm * 60 μm area, the statistics are believed to reveal the general α/β grain size of the obtained material.

Further microstructural details of the obtained material are shown in Fig. 3. Significant Cr partitioning in the β phase can be evidenced via TEM-EDS, as shown in Fig. 3(a). The chemical composition of the α and β phases are reported in Table 4, which shows that the α phase only has a negligible Cr concentration of ~1 wt%, while the β phase presents a ~16 wt% of Cr. This is because Cr is a eutectoid β stabiliser with low or negligible solubility in the α phase [42]. Conversely, it was observed that Sn partitions moderately in the α phase, though it should be noted that we measure a non-negligible 3.7 wt% Sn in the β phase within our alloy (Fig. 3(b)). This corresponds well with the study on Ti-Sn binary alloys [38], which suggests that although Sn is considered a neutral element at

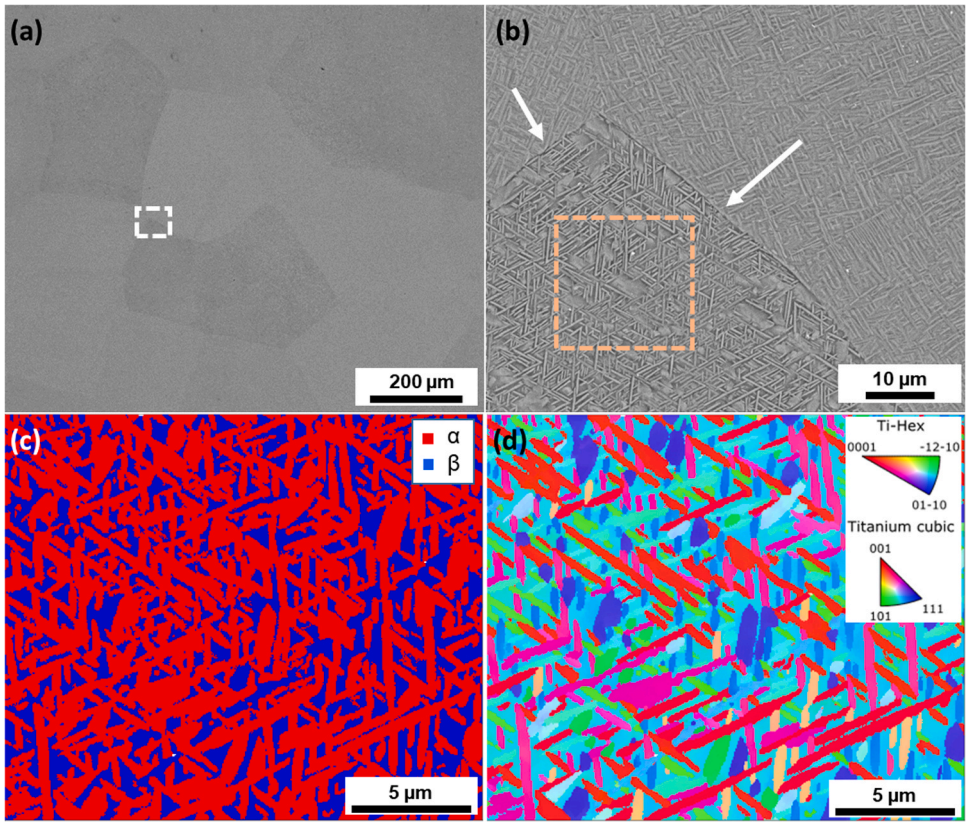

Fig. 2. The Ti-Cr-Sn material studied in this work: (a) secondary electron image showing the quasi-equiaxed morphology of the prior-β grains; the microstructure in the dotted white box was further characterised in (b) evidence that the presence of the continuous grain boundary α, as highlighted via white arrows; the microstructure in the dotted orange box was EBSD scanned via a step size of 100 nm: (c) EBSD phase map showing the basketweave arrangement of the ultra-fine α+ β lamella; (d) IPF-Z map showing the typical hierarchical morphology of the α+ β lamella within the prior-β grain.

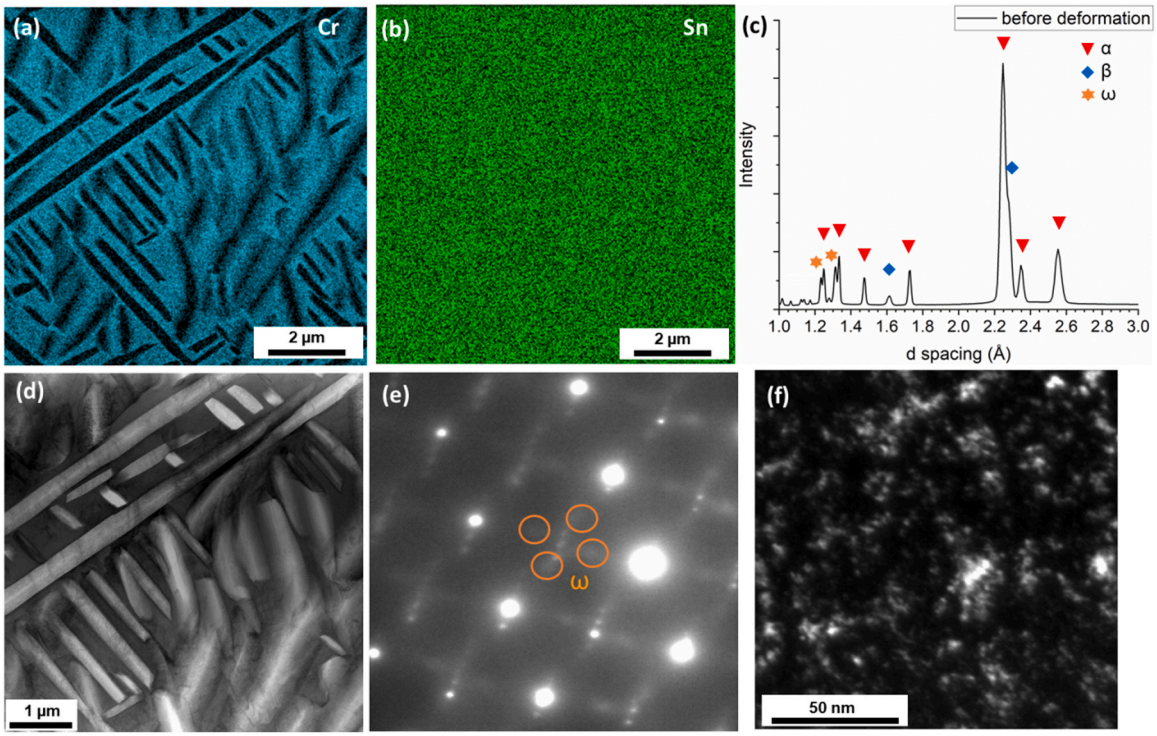

Fig. 3. Significant Cr partitioning was observed in the material via TEM-EDS as shown in (a); TEM-EDS reveals the relatively uniform distribution of Sn as shown in (b); the presence of ω_{iso} in the β phases was evidenced via (c) synchrotron XRD; (d) High-angle annular dark-field (HAADF) STEM image showing the detail features of the ultra-fine α+ β microstructure; the presence of ω_{iso} in the β phases was further evidenced via (e) SAED along the [110]β zone axis and (f) the dark-field diffraction contrast image.

large, it tends to marginally stabilise the α phase when Sn concentration is lower than 8 wt%, resulting in a certain degree of Sn partition in the α phase.

ω precipitates can be identified in the β laths, as evidenced by both synchrotron XRD and STEM shown in Fig. 3. In Fig. 3(c), the ω is demonstrated via the additional peaks around d spacing of 1.2 Å and 1.3 Å. While in the selected area electron diffraction (SAED) patterns ω phase diffraction spots can be observed at the 1/3 < 112 > β and 2/3 < 112 > β position along the [110]β zone axis, forming a symbol of the cross, as highlighted via orange circles in the Fig. 3(e). The presence of ω phase is further characterised via the dark-field diffraction contrast image in Fig. 3(f), which shows that the ω phase is uniformly distributed in the β matrix. The ω observed here is interpreted as isothermal ω_{iso}, considering the fact that it is precipitated during slowing furnace cooling. It is well established that athermal ω_{ath}, the other commonly seen ω in the undeformed microstructure, can only be retained via quenching, which requires a much faster cooling rate than was employed to produce our alloy [28].

A typical hierarchical arrangement of the α lath in the β matrix can also be observed in the STEM image shown in Fig. 3(d). The light contrast of the α phase and the dark appearance of the β matrix in the dark field image further evidence the Cr partitioning. The observed ultra-fine α+ β microstructure suggests that the ω-assisted α nucleation and refinement took place successfully, as per our intended alloy design strategy. In the applied processing route, ω_{iso} phase precipitates during slow cooling [17]. The subsequent α nucleation and growth at the ω/β interface are likely to partially consume the intermediate ω_{iso} phase and promote the diffusion of β stabilisers away from the newly formed α phase [19], which can explain the observed Cr partitioning in the remaining β. The phase transformation pathways leading to the obtained refined microstructure will be further discussed in Section 4.1.

Table 2
Chemical composition of the α and β phase in the Ti-7Cr-4Sn alloy before deformation, measured via TEM-EDS.

wt%	Ti	Cr	Sn
α	Bal.	0.8 ± 0.2	4.4 ± 0.1
β	Bal.	16.2 ± 0.3	3.7 ± 0.1

3.2. Tensile properties

Typical tensile properties of the material investigated here are reported in Table 3, while the corresponding engineering strain-stress curves are displayed in Fig. 4(a). The material exhibits a balanced strength and ductility, with yield stress exceeding 1000 MPa and elongation of approx. 10 %. It also exhibits an extended uniform elongation of around 9 % and a persistent strain hardening behaviour, indicating a satisfactory strain hardening capacity for structural materials, as evidenced further via true strain-stress curves in Fig. 4(b). The fracture surface of tensile tested Ti-7Cr-4Sn is also examined (Appendix A). A ductile fracture is observed, corresponding well with the reported tensile performance. It can be noticed that this alloy has a uniform elongation of around 9 % upon tensile deformation. Although this behaviour is sufficient to be used as a structural material, with a minimum requirement of 5 % uniform elongation, it is significantly lower than that can be achieved in strain transformation metastable Ti alloys. The material only

Table 3
Tensile properties of the ω-assisted α refined Ti-7Cr-4Sn investigated in this study.

Young's modulus E (GPa)	Yield stress σy (MPa)	Ultimate Tensile Strength UTS (MPa)	Elongation ε (%)
109.0 ± 1.6	1067.6 ± 3.9	1136.9 ± 5.3	9.6 ± 0.5

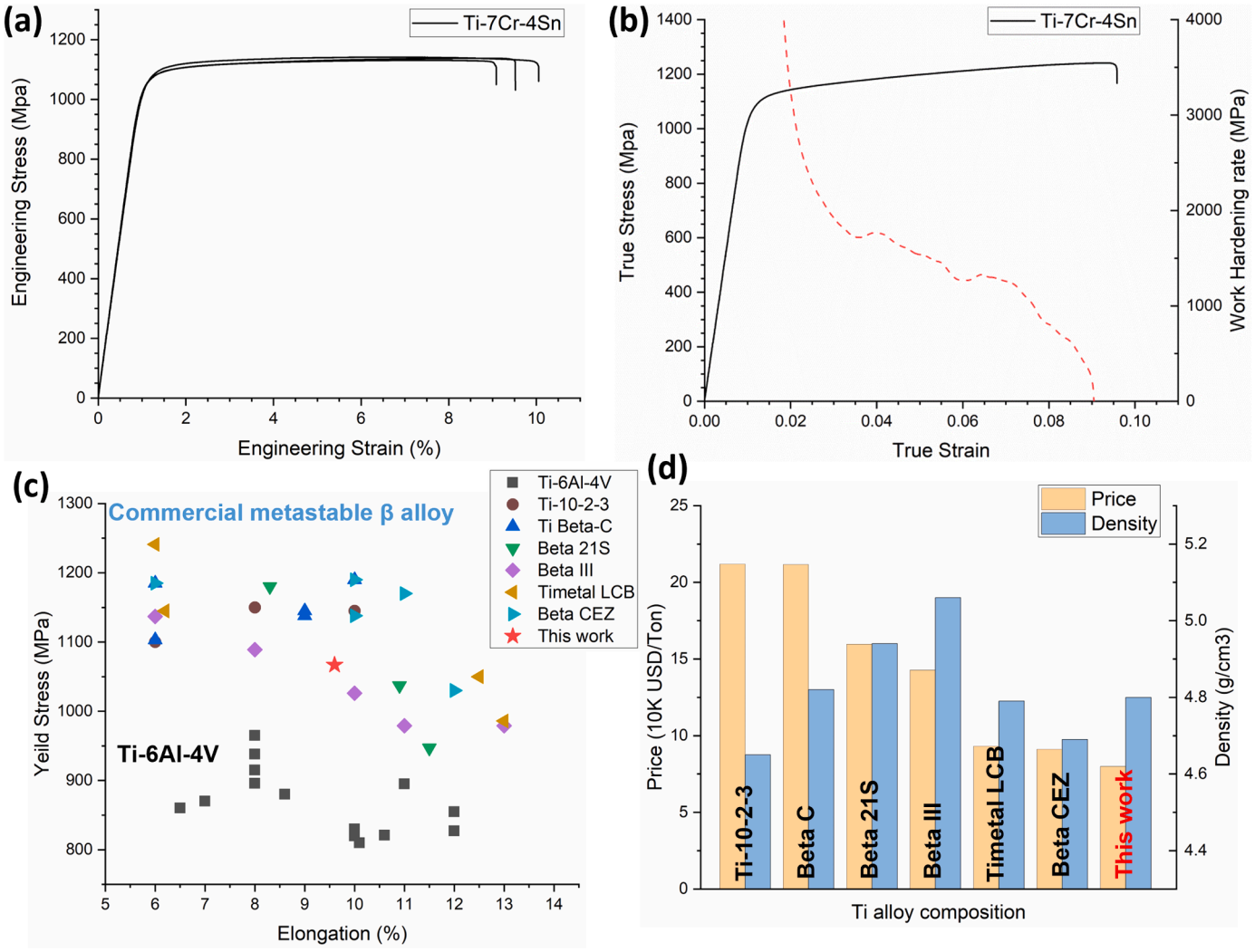

Fig. 4. Tensile performance of the ultra-fine Ti-7Cr-4Sn (a) showing in engineering strain-stress curves; (b) true strain-stress curve and corresponding work hardening rate; (c) for context, these properties are then compared to Ti-6Al-4V and typical commercial metastable β Ti alloys subjected to minimal heat treatment and thermal-mechanical processing [2–4, 35, 42–47]; and (d) the raw material costs and density of the designed alloy compared with typical commercial metastable β Ti alloys [3,36,37].

has a limited working hardening behaviour, and the hardening rate decreases noticeably at a higher strain, leading to the limited uniform elongation of the alloy, which suggests that the deformation slip is likely to be the dominant deformation mechanism. More details will be discussed in Section 4.2.

This strength and ductility performance is superior to the typical cast or hot-rolled Ti-6Al-4V, and comparable to typical commercial metastable β Ti alloys subjected to minimal heat treatment and thermal-mechanical processing, as Fig. 4(c) suggests. As a figure of merit for our alloy, it should be noted that, while our material is simply cooled from the β-transus temperature, some of the comparison alloys shown in Fig. 4(c) underwent costly thermo-mechanical processing. Furthermore, Fig. 4(d) shows the correlation between the raw material cost and the density, compared with typical commercial metastable β Ti alloys. The raw material cost is estimated following the manner reported in similar research [2,8]. It suggests that the proposed alloy, with a moderate density, has a distinguishable advantage in raw material cost.

In addition, specific strength is used to evaluate our alloy compared to Ti-6Al-4V. Based on the material properties summarised in Fig. 4(c), Ti-6Al-4V subjected to minimal heat treatment and thermal-mechanical processing has a tensile strength typically between 900 MPa to 1050 MPa [2–4, 35, 42–47], which means a typical specific strength between 200 and 240 kN·m/kg. Meanwhile, our alloy reported here has a specific strength of 237 kN·m/kg, which compares well with the top-grade performance that can be achieved in Ti-6Al-4V of similar conditions. Regarding the melting point, Ti-6Al-4V has a melting point of 1649 °C, while the estimated melting point of the Ti-7Cr-4Sn alloy is approximately 1627 °C. It is not surprising that these two alloys have similar melting point, since they have similar amounts of Ti (90 wt%), and the melting point of Cr (1907 °C) is very close to that of V (1910°C).

There is a widely accepted apprehension about ω_{iso}, which believes it would significantly embrittle Ti alloy, making it unsuitable for any direct application [24,28]. Therefore, ω_{iso} typically appears in intermediate products for further processing [11,20]. However, this study demonstrates that, via careful composition design and microstructure engineering, balanced properties can be achieved even with the presence of ω_{iso}. Furthermore, it is reasonable to believe that the current material properties can be further improved if additional thermo-mechanical processes are applied, as evidenced in other ω_{iso} related Ti alloys [11,27,48].

3.3. *Microstructure of the obtained material after tensile deformation*

The deformed microstructure after tensile testing was then

characterised in detail to help understand the deformation behaviours in our proposed alloy. Fig. 5(a) suggests that the α and β phase fractions do not undergo any noticeable change after the tensile deformation. High-resolution TKD analysis was performed to characterise the microstructure with precision (Fig. 5(b)). α/β lath with sub-micron thickness and basketweave arrangement is clearly characterised in Fig. 5(c). The significant Cr partitioning remains evident in the deformed microstructure, as shown in Fig. 5(d). The chemical composition of the tensile deformed α and β phases are reported in Table 4, which compared well with those values before tensile deformation, indicating that tensile deformation is a diffusion-less process.

Synchrotron XRD patterns were collected to compare the crystallographic information of the alloy before and after tensile deformation, displayed in Fig. 6(a). It suggests similar α/β phase fractions before and after deformation, corresponding well with the EBSD observation (Fig. 5 (a)). Due to the deformation-induced lattice structure distortion, peak swifts can be observed in the patterns [49,50]. The peak shifts in the deformed β phase are much more subtle than observed in the α phase, suggesting that the α phase accommodates more strain during the tensile deformation [51].

Due to lattice distortion, the ω_{iso} phase is no longer visible in the XRD pattern (Fig. 6(a)), as it is likely that these are masked by the crystallographic peaks of the deformed α phase [28]. However, the presence of ω phase in the deformed β phase is clearly evidenced in the SAED patterns shown in Fig. 6(b). The dark field image in Fig. 6(b) also reveals a high density of dislocations in the deformed β grain structure, suggesting that deformation slip is the main deformation mode in this phase. The observed Cr partitioning is thought to significantly stabilise the β phase (with a calculated Mo_{eq} value of around 20), and upon deformation, there is no evidence of strain-induced phase transformations and twinning in the β phase.

Therefore, the ω precipitates observed in the deformed β phase here should solely interpreted as isothermal ω_{iso}, which is retained from the undeformed material. Although the deformation-induced ω phase can be introduced in the deformed β phase in certain conditions, it is always associated with mechanical twins and generally requires the β phase stability below Mo_{eq} of 15 [28,52], which is not the case in this study.

Table 4
Chemical composition of the tensile deformed α and β phase, measured via TKD-EDS.

wt%	Ti	Cr	Sn
α	Bal.	1.0 ± 0.3	4.5 ± 0.2
β	Bal.	15.6 ± 0.5	3.5 ± 0.3

4. Discussion

4.1. Phase transformation pathways during slowing cooling from single β region

To inform the potential phase transformation pathway, the texture and morphology of the α phase in the β matrix were investigated in detail in the undeformed material. A high-resolution EBSD scan was conducted in an approx. 30 μm * 20 μm area via a step size of 50 nm, displayed in Fig. 7. Two distinctly different morphologies of the α phase can be recognised. One exhibits a short rod shape, as highlighted via white arrows in Fig. 7(a), with a relatively short length and a slight coarsen width. The other exhibits a lengthened thin lath shape, as highlighted via green arrows in Fig. 7(a), with a significantly higher aspect ratio than the former one. The IPF-Z map in Fig. 7(b) also suggests that these two types of α phase have different preferred orientations. These observations indicate that these two types of α phase are most likely precipitated from the parent β phase via different routes.

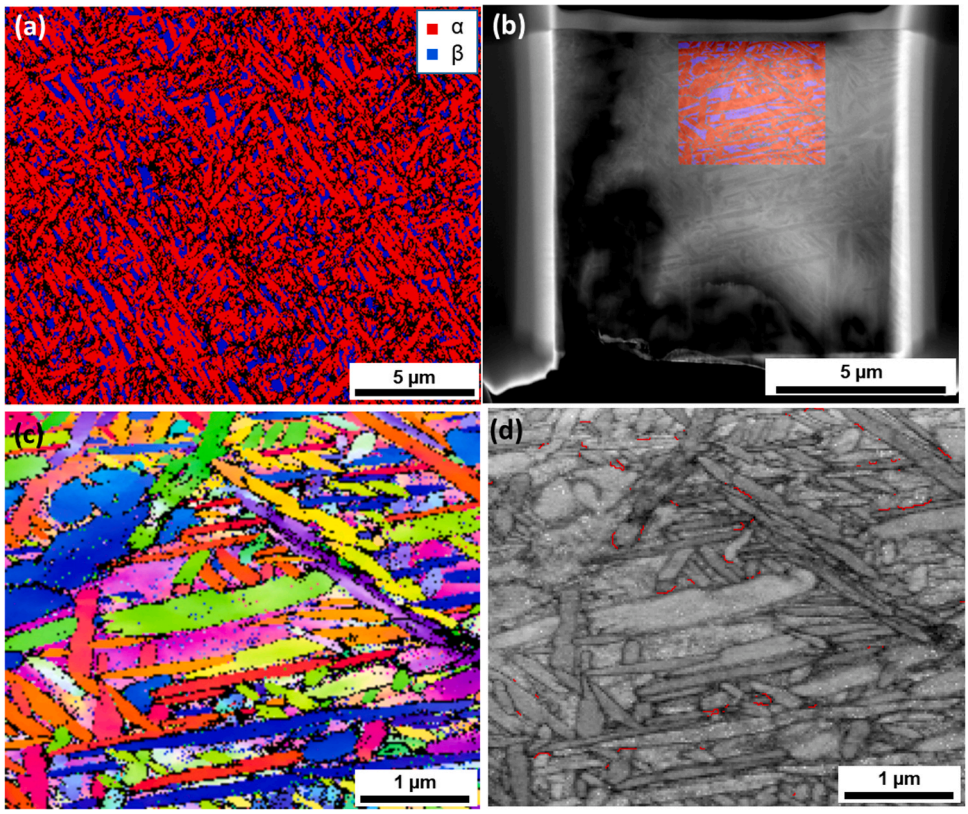

Fig. 5. Microstructure of the tensile deformed Ti-7Cr-4Sn: (a) EBSD phase map reveals a distorted and shattered microstructure; (b) TKD scan conducted on a TEM foil with a step size of 20 nm, overlaid with phase map; (c) TKD IPF-Z map demonstrates the typical deformed texture; (d) significant Cr partitioning can be observed in the deformed material via TKD-EDS.

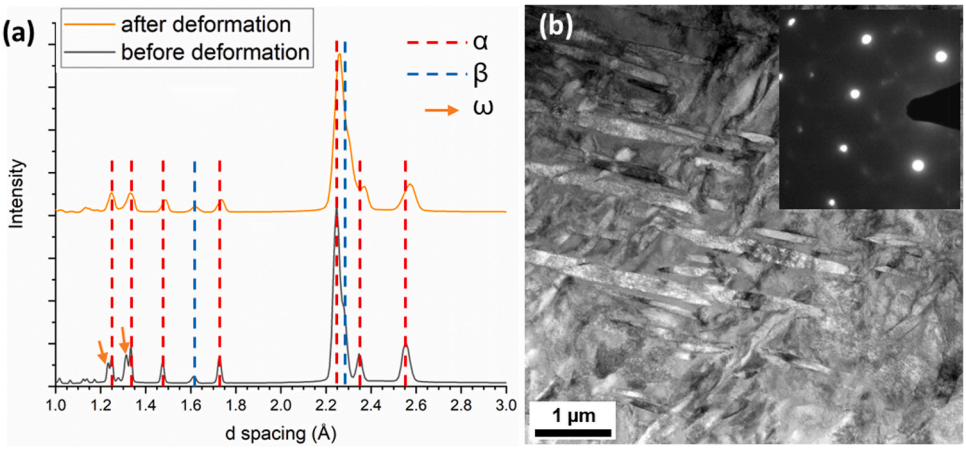

Fig. 6. (a) Synchrotron XRD patterns comparing the crystallographic information of the alloy before and after tensile deformation at break; (b) TEM dark field image after tensile deformation at break and the SAED (insert) along the [110]β zone axis.

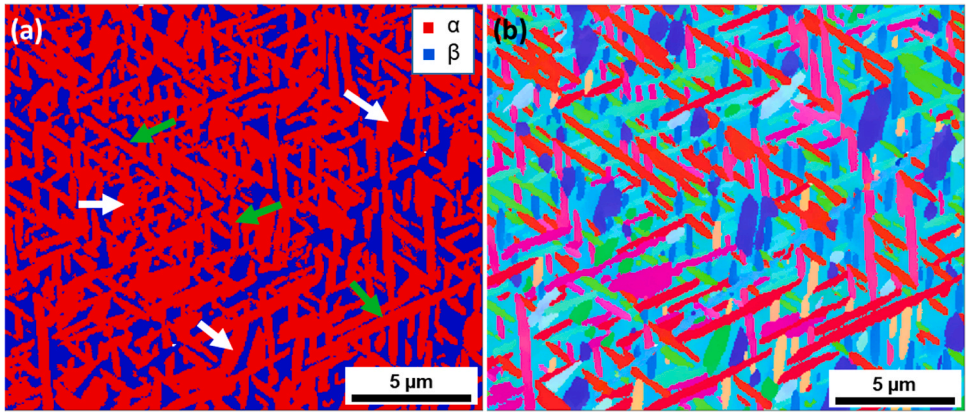

Fig. 7. High-resolution EBSD scan reveals the texture and crystallographic arrangements of the α phase in the undeformed β matrix, in (a) phase map and (b) IPF-Z Map. Two distinctly different morphologies of the α phase can be recognised. The short rod shape α is highlighted via white arrows, and the lengthened thin lath shape α is highlighted via green arrows.

Further experimental evidence to inform the potential phase transformation pathway is reported in Fig. 8. To investigate the initial α formation at the temperature of just below β transus, the material was near-equilibrium treated at 800°C followed by water quenching. The EBSD phase map in Fig. 8(a) exhibits the remaining alpha phases that have not yet been dissolved at such a temperature. The increased thermal stability of these alpha phases indicates they are likely to be the first alpha phases that form during cooling from β transus [53,54]. Since the observed alpha phases are located both at the grain boundary and inside the β grains, it can assumed that the grain boundary α (α_{GB}) and primary α (α_P) are likely to be precipitated almost simultaneously once the temperature drops down from the β transus.

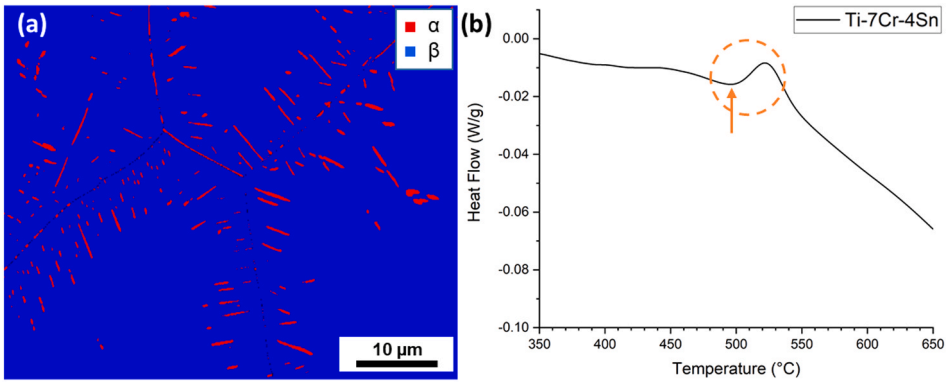

Fig. 8. Further experimental evidence to inform the potential phase transformation pathway: (a) EBSD phase map of the material that near-equilibrium treated at 800°C followed by water quenching, revealing the initial α formation at the temperature just below β transus; (b) SDT analysis of the material in the temperature range from 350°C to 650°C, the starting temperature of ω_{iso} precipitation is indicated by the noticeable change of the heat flow pattern around the 500°C, as highlighted by the orange circle and arrow.

On the other hand, the ω_{iso} precipitation and related phase transformations are known to occur at a much lower temperature [19,20]. SDT analysis suggests the ω_{iso} in the room temperature material will fully dissolve at around 500°C, as indicated by the noticeable change in the heat flow pattern, pointed out by the orange circle and arrow in Fig. 8(b). It corresponds well with the literature that ω_{iso} rarely retained above 550°C [28]. It can be assumed that the starting temperature of ω_{iso} precipitation of the studied material during cooling should also be at a similar temperature.

Therefore, phase transformation pathways are proposed and schematically illustrated in Fig. 9. Since the material is cooled from a temperature above the β transus, the initial microstructure is a full β phase microstructure, as indicated in Fig. 9(a). When the temperature drops through the β transus, the α phase starts to precipitate in the β matrix with lattice defects as the preferred precipitation sites [55]. It would lead to the formation of grain boundary α (α_{GB}) at the prior-β grain boundaries and primary α (α_P) within the prior-β grains [56], as evidenced in Fig. 8(a) and illustrated in Fig. 9(b). Since both α_{GB} and α_P are formed via β → α pathway, their precipitation should obey the Burgers orientation relationship (OR) {110}β // {0001}α, $<111>_\beta$ // $<11\bar{2}0>_\alpha$ [57,58].

The formation and growth of α_{GB} and α_P would expel the β stabiliser into the β matrix [19], leading to β matrix with a Cr concentration higher than the initial 7 % at a temperature lower than β transus. However, it could not fully stabilise the β matrix to suppress the ω_{iso} precipitation, since the room temperature β phase only has a Mo_{eq} value of about 20.

Further along the furnace cooling, it is believed that the ω_{iso} would start to precipitate when the temperature drops slightly below 500°C, as evidenced in Fig. 8(b) and illustrated in Fig. 9(c). Research suggests that such precipitation should follow the Silcock OR, where {111}β // {0001}ω, $<011>_\beta$ // $<1\bar{2}10>_\omega$ [20]. It is also well known that the ω_{iso} precipitates homogeneously in the β matrix, and the β → ω transformation is preferred over the β → α transformation [28,43]. Therefore, the α_p formation would most likely be suppressed after this point.

Although at a relatively low temperature below 500°C, another type of α phase, the secondary α (α_s), should still be able to precipitate at the ω/β interface via the well-established ω_{iso} assisted α formation pathway (β → ω → α), as illustrated in Fig. 9(d). In recent studies, such α precipitation has been experimentally observed in Ti-5553 alloy at 375°C without any holding time [20] and in Ti-7333 alloy at 400°C with a limited holding time of less than 5 min [11]. Both studies also suggested that the starting temperature for ω_{iso} assisted α nucleation should be slightly above 350°C [11,20]. Therefore, it can be assumed that during the furnace cooling in this study, ω_{iso} assisted α_s nucleation is likely to take place in the temperature range from 500°C to 350°C. Indeed, during the processing of our material, the cooling phase within such a temperature range lasted about 3–4 hours, allowing presumably enough time for α_s to nucleate and grow.

Research suggests the ω_{iso} assisted α still follows the Burgers OR to the parent β [20]. However, due to the different phase transformation routes of α_p and α_s, their preferred variant selection would likely differ, leading to different preferred orientations.

The homogenise distributed ω_{iso} provides abundant precipitation sites for α_s, more than that for the α_p, as the latter mainly precipitates at intrinsic metal defects [19,24]. Furthermore, the Ti-Cr is known to be a high misfit system, which would further promote ω precipitation and the α nucleation at the ω/β interface [43]. As a result, a significant amount of α_s will be introduced into the β matrix. The competitive growth between different α phases (including both α_p and α_s) and the β phase is believed to result in the final ultra-fine microstructure. The short rod shape α observed in the room temperature material is likely to be the α_p, as it has a longer growth time during cooling. While the lengthened thin lath shape α is likely to be the α_s, as the ω_{iso} assisted α nucleation tends to form a needle-like morphology with a high aspect ratio [19,20]. It can be assumed that the further growth of ω_{iso} assisted α_s phase would most likely maintain such a feature.

4.2. Origins of the observed ductility

Experimental evidence in Section 3.3 suggests that dislocation slip should be the dominant deformation mechanism of the proposed alloy, while the α phase accommodates more strain during the tensile deformation. Since Cr is strongly partitioned in the β phase and α stabiliser is not added to the alloy, a solute lean α phase is obtained in the material, as evidenced by the EDS results. Further analysis of the EBSD data reported in Fig. 2, as displayed in Fig. 10 (a), reveals that the obtained solute lean α phase has a particular preferred crystallographic arrangement, with the prevalent misorientation between neighbouring α phases is $[11\bar{2}0]/60°$. Such an arrangement is widely considered the preferred misorientation configuration between the neighbouring α-variants, as it is close to $\{10\bar{1}1\} <10\bar{1}2>$twining, possessing lower energy [59]. Therefore, compared to other misorientation configurations of the phase boundary, it is an energetically preferred configuration for dislocation movement, which helps to improve the overall ductility of the α phase [60]. Meanwhile, prior research suggests that, for α variants with a higher presence of α stabiliser (for example, Ti-6Al-4V), $[\bar{1}0553]/63.26°$ tends to take over and become the predominate misorientation configuration, which tends to compromise the material's ductility [60,61].

About 4.5 wt% Sn is retained in the α phase. In terms of α phase stabilisation effects, 4.5 wt% Sn equates to 1.5 wt% Al_{eq} [62]. Prior research evidenced that such limited amounts of α stabilisers do not influence the strain-stability of the α phase [63]. Studies on Ti-Al binary alloys suggests that, for Al addition less than or equal to 3 wt%, Ti-Al alloys exhibit similar deformation behaviour to pure Ti, with very ductile performance and slightly enhanced $\{10\bar{1}2\}<\bar{1}011>$ twins [63]. Therefore, we can assume that the α phase in our alloy deforms similarly to that. Indeed, occasional $\{10\bar{1}2\}<\bar{1}011>$ twins can be identified

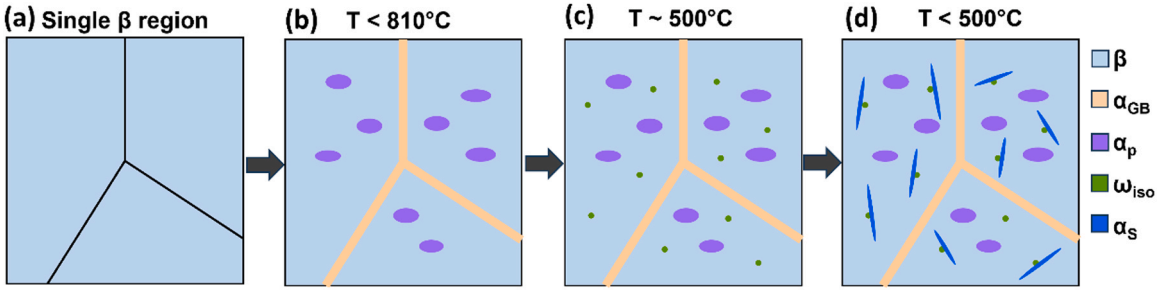

Fig. 9. Schematic drawing illustrating the phase transformation pathway and the microstructure evolution during the slowing cooling. (a) full β phase microstructure when temperature above the β transus; (b) grain boundary α (α_{GB}) and primary α (α_P) start to precipitate from the β matrix when the temperature drops through the β transus; (c) isothermal ω (ω_{iso}) starts to precipitate from the β matrix at a temperature around 500°C, which suppress further α_P formation; (d) at temperature below 500°C, the secondary α (α_s) will precipitate at the ω/β interface via the well-established ω_{iso} assisted α formation pathway.

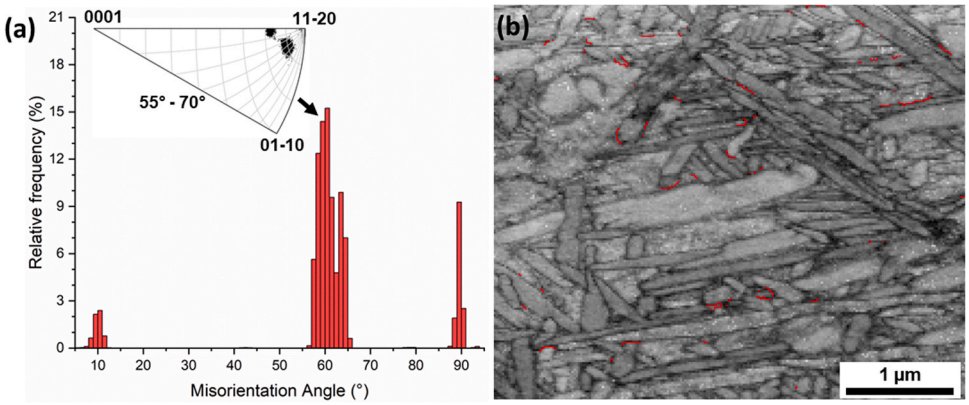

Fig. 10. The solute lean α phase exhibits a favourable crystallographic arrangement and deformation behaviour: (a) EBSD analyses of the crystallographic arrangements suggesting the prevalent misorientation between neighbouring α phases is [11$\bar{2}$0]/60°; (b) TKD band contrast showing the {10$\bar{1}$2}<$\bar{1}$011 > twinning boundary within the deformed α phase, as highlighted via the red lines.

within the deformed α phase, as highlighted via the twin boundary mapped in the TKD band contrast image, as shown in Fig. 10 (b). Such twin boundary has a misorientation configuration of [11$\bar{2}$0]/84.8°, which can not be identified in the undeformed material (Fig. 10(a)). Therefore, it is most likely the result of tensile deformation.

Due to the submicron dimension of the α-grains in the alloy, only limited twin activity is observed, as the grain size is known to significantly affect the activation of twinning behaviours in α-titanium [64]. Albeit limited in presence, twinning effectively provides an alternative deformation mechanism from the dominant deformation slip, contributing to an increase in the ductility of the α phase.

Since the presence of the ω_{iso} phase is known to embrittle the β phase [28,48], a balanced α/β phase ratio with α phase in dominance seems to be crucial for obtaining a ductile alloy in these ternary systems. In this study, only approx. 30 % of β was reserved in the room-temperature microstructure. In other studies investigating the role of eutectoid stabilisers on the tensile performance of Ti alloys, where a much higher amount of β phase is retained, microstructures tend to have brittle characteristics, with typical elongation less than 5 % [25,27].

The presence of α_{GB}, and more precisely, the thickness of α_{GB}, is known to significantly influence the ductility of the Ti alloy [65]. Coarse α_{GB} are thought to be crucial in embrittling ω-assisted α refined microstructures, as these microstructural features might provide a pathway for crack propagation [11,24]. In cases where a notable amount of α stabiliser is used to formulate the alloy, the ω formation would reject the α stabiliser, which then concentrates at the prior-β grain boundaries, leading α_{GB} coarsening [11]. Since in our alloy limited α stabilisers are used (approx. 1.5 Al_{eq}), α_{GB} remains fine within the sub-micron range, which prior research suggests will have no detrimental effect on ductility [65].

4.3. Origins of the observed strength

Compared to the material's ductility, the high strength achieved in ω assisted α refined ultra-fine material has been investigated more thoroughly over the past 10 years [11,17,24,25].

The high strength observed in the alloy can be ascribed to multiple factors. It is well established that the ultra-fine grain size leads to a high density of the phase boundaries, which improves boundary strengthening, as loosely explained by the Hall-Petch relationship [66,67]. In addition, the reserve of nanoscale ω_{iso} precipitates found in the β phase would increase the alloy strength through precipitation hardening mechanisms and by inducing strain gradients near phase boundaries [17]. These two factors are generally considered the major contributors to the strength [2,24].

Additionally, the basketweave arrangement of the α/β lath and solution strengthening is believed to help promote the material's strength [66,68]. It is noteworthy that research suggests Sn as one of the most effective solid solution strengtheners in the β phase [39]. The presence of approx. 3.7 wt% Sn in the β phase will further help to improve the material's strength.

5. Conclusion

In this study, we have demonstrated how a ternary alloy based on eutectoid β and neutral stabilisers (i.e. Ti-7Cr-4Sn), can form an ultra-fine microstructure and exhibit a desirable combination of strength and ductility after primary processing. Using this specific alloy as a model alloy, it is demonstrated that microstructure and mechanical properties are influenced by the specific partitioning of the elements and α/ω phase precipitation during a slow cooling from the β phase. The results suggest a novel alloy design strategy to obtain low-cost Ti alloys with superior mechanical properties. These findings could be extended to develop other novel Ti alloys based on eutectoid constitutions, opening up new avenues for research in the metallurgy of Ti alloys beyond traditional aerospace grades.

From the present study, the following conclusions can be drawn:

1. After slow furnace cooling, the proposed Ti-7Cr-4Sn alloy has an ultra-fine microstructure of α/β laths within the sub-micron range, and nanoscale ω participates. Strong Cr segregation can be identified in the β phase, while slight partitioning of Sn can be observed between α and β phase.
2. The material exhibits an excellent combination of strength and ductility comparable to typical commercial metastable β Ti alloys, while having a distinguishable advantage in material cost.
3. Different microstructure features, including grain boundary α (α_{GB}), short rod shape primary α (α_P), isothermal ω (ω_{iso}) and ω assisted secondary α (α_s) are precipitated from β matrix in different stages of cooling. The competitive growth between different α phases (including both α_p and α_s) and the β phase is believed to result in the final ultra-fine microstructure.
4. Dislocation slip is the dominant deformation mechanism of the proposed alloy, with the presence of occasional {10$\bar{1}$2}<$\bar{1}$ 011 > twins within the deformed α phase.
5. The ductility of the proposed alloy is mainly attributed to the preferred crystallographic arrangement between neighbouring solute-lean α variants, the ductile nature of the solute-lean α phase, a balanced α/β phase ratio with α phase in dominance and fine α_{GB} within the sub-micron range.
6. The strength of the proposed alloy is mainly attributed to the ultra-fine grain size, precipitation hardening of the nanoscale ω

precipitates, the basketweave arrangement of the α/β lath and solution strengthening of the alloying elements.

CRediT authorship contribution statement

McWilliams Brandon: Writing – review & editing, Formal analysis, Conceptualization. **Dunstan Matthew K:** Writing – review & editing, Formal analysis, Conceptualization. **Zou Zhiyi:** Writing – original draft, Methodology, Investigation, Formal analysis, Conceptualization. **Simonelli Marco:** Writing – review & editing, Resources, Methodology, Formal analysis, Conceptualization. **Hague Richard:** Writing – review & editing, Resources, Conceptualization. **Robertson Stuart:** Writing – review & editing, Investigation, Formal analysis.

Declaration of Competing Interest

The authors declare that they have no known competing financial interests or personal relationships that could have appeared to influence the work reported in this paper.

Acknowledgements

The work presented here has been made possible by funding supported by the U.S.A. Army Research Office (grant W911NF2120202) and Engineering and Physical Sciences Research Council (EPSRC), UK (grant EP/P031684/1). The authors acknowledge the use of facilities within the Loughborough Materials Characterisation Centre and for access to the Helios PFIB, funded by the EPSRC grant EP/P030599/1.

Appendix A. Fracture surface of tensile tested Ti-7Cr-4Sn

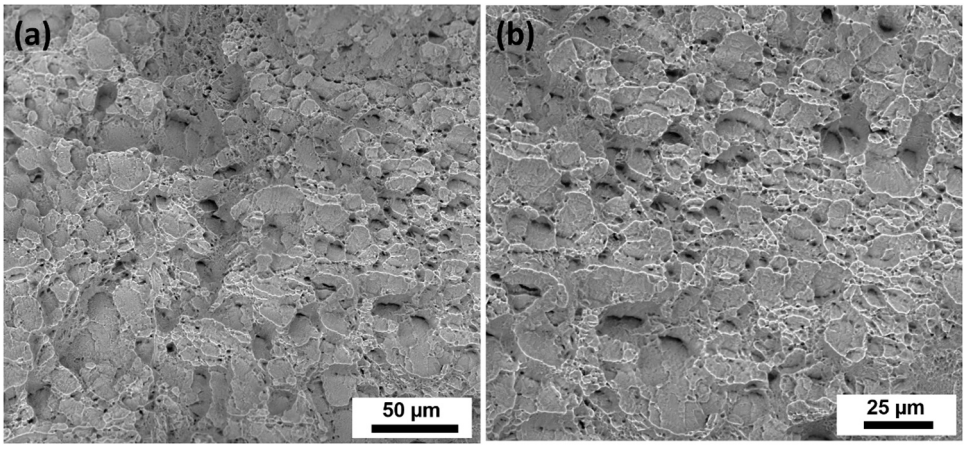

Figure A.1. The Fracture surface of the tensile tested Ti-7Cr-4Sn observed under (a) x500 magnification and (b) x800 magnification. The fracture surface is covered with dimples of different sizes. Such a fracture surface is generally formed due to shear deformation under sliding mode, which suggests a ductile fracture of the material

Data availability

The data that support the findings of this study are available from the corresponding author, Marco Simonelli, upon reasonable request.

References

[1] Q. Zhao, Q. Sun, S. Xin, Y. Chen, C. Wu, H. Wang, J. Xu, M. Wan, W. Zeng, Y. Zhao, High-strength titanium alloys for aerospace engineering applications: a review on melting-forging process, Mater. Sci. Eng.: A 845 (2022) 143260.
[2] H. Zhang, J. Zhang, J. Hou, D. Zhang, Y. Yue, G. Liu, J. Sun, Making a low-cost duplex titanium alloy ultra-strong and ductile via interstitial solutes, Acta Mater. 241 (2022) 118411.
[3] M.J. Donachie, Titanium: a technical guide, ASM International, Materials Park, United States, 2000.
[4] M.O. Bodunrin, L.H. Chown, J.A. Omotoyinbo, Development of low-cost titanium alloys: A chronicle of challenges and opportunities, Mater. Today.: Proc. 38 (2021) 564–569.
[5] A. Gupta, R. Khatirkar, J. Singh, A review of microstructure and texture evolution during plastic deformation and heat treatment of β-Ti alloys, J. Alloy. Compd. 899 (2022) 163242.
[6] C. Cui, B. Hu, L. Zhao, S. Liu, Titanium alloy production technology, market prospects and industry development, Mater. Des. 32 (2011) 1684–1691.
[7] J.M. Oh, C.H. Park, J.-T. Yeom, J.-K. Hong, N. Kang, S.W. Lee, High strength and ductility in low-cost Ti–Al–Fe–Mn alloy exhibiting transformation-induced plasticity, Mater. Sci. Eng.: A 772 (2020) 138813.
[8] C. Zhang, X. Bao, M. Hao, W. Chen, D. Zhang, D. Wang, J. Zhang, G. Liu, J. Sun, Hierarchical nano-martensite-engineered a low-cost ultra-strong and ductile titanium alloy, Nat. Commun. 13 (2022) 5966.
[9] C. Zhu, X.-y Zhang, C. Li, C. Liu, K. Zhou, A strengthening strategy for metastable β titanium alloys: synergy effect of primary α phase and β phase stability, Mater. Sci. Eng.: A 852 (2022) 143736.
[10] T. Zhang, J. Zhu, T. Yang, J. Luan, H. Kong, W. Liu, B. Cao, S. Wu, D. Wang, Y. Wang, C.-T. Liu, A new α + β Ti-alloy with refined microstructures and enhanced mechanical properties in the as-cast state, Scr. Mater. 207 (2022) 114260.
[11] R. Dong, J. Li, H. Kou, J. Fan, Y. Zhao, H. Hou, L. Wu, ω-Assisted refinement of α phase and its effect on the tensile properties of a near β titanium alloy, J. Mater. Sci. Technol. 44 (2020) 24–30.
[12] C.-c Liu, Y.-h-z Li, J. Gu, M. Song, Phase transformation in titanium alloys: A review, Trans. Nonferrous Met. Soc. China 34 (2024) 3093–3117.
[13] X. Bao, W. Chen, J. Zhang, Y. Yue, J. Sun, Achieving high strength-ductility synergy in a hierarchical structured metastable β-titanium alloy using through-transus forging, J. Mater. Res. Technol. 11 (2021) 1622–1636.
[14] Y. Jia, H. Su, S. Cao, R. Shi, Y. Ma, Q. Wang, S. Huang, R. Zhang, Q. Hu, Y. Zheng, S. Zheng, J. Lei, R. Yang, Fabrication of highly heterogeneous precipitate microstructure in an α/β titanium alloy, Acta Mater. 279 (2024) 120302.
[15] X. Zhu, Q. Fan, H. Gong, J. Ying, H. Yu, X. Cheng, L. Yang, L. Yang, N. Li, J. Li, Achieving super-high strength and acceptable plasticity for a near β-type Ti-4.5Mo-5.1Al-1.8Zr-1.1Sn-2.5Cr-2.9Zn alloy through manipulating hierarchical microstructure, Mater. Sci. Eng.: A 825 (2021) 141907.
[16] K. Wang, D. Wu, D. Wang, Z. Deng, Y. Tian, L. Zhang, L. Liu, Influence of cooling rate on ω phase precipitation and deformation mechanism of a novel metastable β titanium alloy, Mater. Sci. Eng.: A 829 (2022) 142151.
[17] F. Zhang, J. Feng, W. Xiang, Q. Fu, W. Yuan, Enhanced mechanical properties in metastable β titanium alloy via ω-assisted nucleation, Mater. Sci. Eng.: A 858 (2022) 144082.
[18] Y. Zhang, S. Xiang, Y.B. Tan, X.M. Ji, Study on ω-assisted α nucleation behavior of metastable β-Ti alloys from phase transformation mechanism, J. Alloy. Compd. 890 (2022) 161686.

[19] Y. Zheng, R.E.A. Williams, J.M. Sosa, T. Alam, Y. Wang, R. Banerjee, H.L. Fraser, The indirect influence of the ω phase on the degree of refinement of distributions of the α phase in metastable β-Titanium alloys, Acta Mater. 103 (2016) 165–173.
[20] Y. Zheng, R.E.A. Williams, D. Wang, R. Shi, S. Nag, P. Kami, J.M. Sosa, R. Banerjee, Y. Wang, H.L. Fraser, Role of ω phase in the formation of extremely refined intragranular α precipitates in metastable β-titanium alloys, Acta Mater. 103 (2016) 850–858.
[21] R. Dong, H. Kou, L. Wu, L. Yang, Y. Zhao, H. Hou, to ω transformation strain associated with the precipitation of α phase in a metastable β titanium alloy, J. Mater. Sci. 56 (2021) 1685–1693.
[22] C.E.P. Talbot, N.L. Church, N.G. Jones, Observation of α phase nucleation within ω precipitates with novel orientation relationship in a low misfit metastable β-Ti alloy through EBSD, Scr. Mater. 255 (2025) 116335.
[23] N.G. Jones, R.J. Dashwood, M. Jackson, D. Dye, β Phase decomposition in Ti–5Al–5Mo–5V–3Cr, Acta Mater. 57 (2009) 3830–3839.
[24] R. Zhang, Y. Ma, M. Qi, S. Huang, S.S. Youssef, G. Xi, J. Qiu, J. Lei, R. Yang, P. Wang, The effect of precursory α and ω phase on microstructure evolution and tensile properties of metastable β titanium alloy, J. Mater. Res. Technol. 16 (2022) 912–921.
[25] B. Song, W. Xiao, Y. Fu, C. Ma, L. Zhou, Role of nanosized intermediate phases on α precipitation in a high-strength near β titanium alloy, Mater. Lett. 275 (2020) 128147.
[26] J. Gupta, I.K. Jha, R.K. Khatirkar, J. Singh, Effect of aging on tensile and fracture behavior of a metastable Ti-15 V–3Cr–3Al–3Sn β-titanium alloy, J. Alloy. Compd. 1004 (2024) 175803.
[27] S. Sadeghpour, S.M. Abbasi, M. Morakabati, S. Bruschi, Correlation between alpha phase morphology and tensile properties of a new beta titanium alloy, Mater. Des. 121 (2017) 24–35.
[28] J. Ballor, T. Li, F. Prima, C.J. Boehlert, A. Devaraj, A review of the metastable omega phase in beta titanium alloys: the phase transformation mechanisms and its effect on mechanical properties, Int. Mater. Rev. 68 (2023) 26–45.
[29] S. Pilz, A. Hariharan, F. Günther, M. Zimmermann, A. Gebert, Influence of isothermal omega precipitation aging on deformation mechanisms and mechanical properties of a β-type Ti-Nb alloy, J. Alloy. Compd. 930 (2023) 167309.
[30] M.S. Park, W.-T. Chiu, N. Nohira, M. Tahara, H. Hosoda, Effects of Cr and Sn additives on the martensitic transformation and deformation behavior of Ti-Cr-Sn biomedical shape memory alloys, Mater. Sci. Eng.: A 822 (2021) 141668.
[31] C. Brozek, F. Sun, P. Vermaut, Y. Millet, A. Lenain, D. Embury, P.J. Jacques, F. Prima, A β-titanium alloy with extra high strain-hardening rate: Design and mechanical properties, Scr. Mater. 114 (2016) 60–64.
[32] W.T. Chiu, K. Wakabayashi, A. Umise, M. Tahara, T. Inamura, H. Hosoda, Enhancement of the shape memory effect by the introductions of Cr and Sn into the β–Ti alloy towards the biomedical applications, J. Alloy. Compd. 875 (2021) 160088.
[33] N.L. Okamoto, F. Brumbauer, M. Luckabauer, W. Sprengel, R. Abe, T. Ichitsubo, Why is neutral tin addition necessary for biocompatible β-titanium alloys?–Synergistic effects of suppressing ω transformations, Acta Mater. 273 (2024) 119968.
[34] W. Abd-Elaziem, M.A. Darwish, A. Hamada, W.M. Daoush, Titanium-Based alloys and composites for orthopedic implants applications: a comprehensive review, Mater. Des. 241 (2024) 112850.
[35] L. Kang, C. Yang, A review on high-strength titanium alloys: microstructure, strengthening, and properties, Adv. Eng. Mater. 21 (2019) 1801359.
[36] S.M. Market, Shanghai Metals Market, in.
[37] L.M. Exchange, London Metal Exchange, in.
[38] H. Okamoto, Sn-Ti (Tin-Titanium), J. Phase Equilibria Diffus. 31 (2010) 202–203.
[39] G.H. Zhao, X.Z. Liang, B. Kim, P.E.J. Rivera-Díaz-del-Castillo, Modelling strengthening mechanisms in beta-type Ti alloys, Mater. Sci. Eng.: A 756 (2019) 156–160.
[40] Z. Zou, M.K. Dunstan, B. McWilliams, R. Hague, M. Simonelli, Identification of an affordable and printable metastable β Ti alloy with outstanding deformation behaviour for use in laser powder bed fusion, Mater. Sci. Eng.: A 902 (2024) 146619.
[41] A.S.T.M. I, A.S.T.M. E8/E8M-16a, Standard Test Methods for Tension Testing of Metallic Materials, ASTM International, West Conshohocken, PA, USA, 2016.
[42] I. Polmear, Light alloys: from traditional alloys to nanocrystals, Butterworth-Heinemann, 2005.
[43] G. Lütjering, J.C. Williams, Titanium, Springer Science & Business Media, 2007.
[44] Y. Kosaka, S.P. Fox, K. Faller, S.H. Reichman, Properties and processing ofTIMETAL LCB, J. Mater. Eng. Perform. 14 (2005) 792–798.
[45] G. Welsch, R. Boyer, E. Collings, Materials properties handbook: titanium alloys, ASM international, 1993.
[46] I. Weiss, S.L. Semiatin, Thermomechanical processing of beta titanium alloys—an overview, Mater. Sci. Eng.: A 243 (1998) 46–65.
[47] N. Yumak, K. Aslantaş, A review on heat treatment efficiency in metastable β titanium alloys: the role of treatment process and parameters, J. Mater. Res. Technol. 9 (2020) 15360–15380.
[48] W. Wang, X. Zhang, W. Mei, J. Sun, Role of omega phase evolution in plastic deformation of twinning-induced plasticity β Ti–12V–2Fe–1Al alloy, Mater. Des. 186 (2020) 108282.
[49] M. Chen, S. Van Petegem, Z. Zou, M. Simonelli, Y.Y. Tse, C.S.T. Chang, M. G. Makowska, D.Ferreira Sanchez, H. Moens-Van Swygenhoven, Microstructural engineering of a dual-phase Ti-Al-V-Fe alloy via in situ alloying during laser powder bed fusion, Addit. Manuf. 59 (2022) 103173.
[50] W. Xu, E.W. Lui, A. Pateras, M. Qian, M. Brandt, In situ tailoring microstructure in additively manufactured Ti-6Al-4V for superior mechanical performance, Acta Mater. 125 (2017) 390–400.
[51] D. Zhang, L. Wang, H. Zhang, A. Maldar, G. Zhu, W. Chen, J.-S. Park, J. Wang, X. Zeng, Effect of heat treatment on the tensile behavior of selective laser melted Ti-6Al-4V by in situ X-ray characterization, Acta Mater. 189 (2020) 93–104.
[52] S.A. Mantri, D. Choudhuri, T. Alam, V. Ageh, F. Sun, F. Prima, R. Banerjee, Change in the deformation mode resulting from beta-omega compositional partitioning in a TiMo alloy: Room versus elevated temperature, Scr. Mater. 130 (2017) 69–73.
[53] F.R. Kaschel, R.K. Vijayaraghavan, A. Shmeliov, E.K. McCarthy, M. Canavan, P. J. McNally, D.P. Dowling, V. Nicolosi, M. Celikin, Mechanism of stress relaxation and phase transformation in additively manufactured Ti-6Al-4V via in situ high temperature XRD and TEM analyses, Acta Mater. 188 (2020) 720–732.
[54] A.L. Pilchak, G.A. Sargent, S.L. Semiatin, Early stages of microstructure and texture evolution during beta annealing of Ti-6Al-4V, Met. Mat. Trans. A (2017).
[55] J. Haubrich, J. Gussone, P. Barriobero-Vila, P. Kürnsteiner, E.A. Jägle, D. Raabe, N. Schell, G. Requena, The role of lattice defects, element partitioning and intrinsic heat effects on the microstructure in selective laser melted Ti-6Al-4V, Acta Mater. 167 (2019) 136–148.
[56] R. Shi, V. Dixit, H.L. Fraser, Y. Wang, Variant selection of grain boundary α by special prior β grain boundaries in titanium alloys, Acta Mater. 75 (2014) 156–166.
[57] W.G. Burgers, On the process of transition of the cubic-body-centered modification into the hexagonal-close-packed modification of zirconium, Physica 1 (1934) 561–586.
[58] N. Stanford, P.S. Bate, Crystallographic variant selection in Ti–6Al–4V, Acta Mater. 52 (2004) 5215–5224.
[59] S.C. Wang, M. Aindow, M.J. Starink, Effect of self-accommodation on α/α boundary populations in pure titanium, Acta Mater. 51 (2003) 2485–2503.
[60] T. Song, Z. Chen, X. Cui, S. Lu, H. Chen, H. Wang, T. Dong, B. Qin, K.C. Chan, M. Brandt, X. Liao, S.P. Ringer, M. Qian, Strong and ductile titanium–oxygen–iron alloys by additive manufacturing, Nature 618 (2023) 63–68.
[61] H.Z. Zhong, Z. Liu, J.F. Gu, The vertical and triangular morphology in the as-deposited Ti-6Al-4V, Mater. Charact. 131 (2017) 91–97.
[62] R.P. Kolli, W.J. Joost, S. Ankem, Phase stability and stress-induced transformations in beta titanium alloys, JOM 67 (2015) 1273–1280.
[63] A. Fitzner, D.G.L. Prakash, J.Q. da Fonseca, M. Thomas, S.-Y. Zhang, J. Kelleher, P. Manuel, M. Preuss, The effect of aluminium on twinning in binary alpha-titanium, Acta Mater. 103 (2016) 341–351.
[64] B. Wang, H. Liu, Y. Zhang, B. Zhou, L. Deng, C. Wang, J. Chen, Y. Zhang, Effect of grain size on twinning behavior of pure titanium at room temperature, Mater. Sci. Eng.: A 827 (2021) 142060.
[65] K.N. Kumar, P. Muneshwar, S.K. Singh, A.K. Jha, B. Pant, K.M. George, Effect of grain boundary alpha on mechanical properties of Ti5.4Al3Mo1V Alloy, JOM 67 (2015) 1265–1272.
[66] M. Simonelli, Z. Zou, P. Barriobero-Vila, Y.Y. Tse, The development of ultrafine grain structure in an additively manufactured titanium alloy via high-temperature microscopy, Materialia 30 (2023) 101856.
[67] F.J. Gil, M.P. Ginebra, J.M. Manero, J.A. Planell, Formation of α-Widmanstätten structure: effects of grain size and cooling rate on the Widmanstätten morphologies and on the mechanical properties in Ti6Al4V alloy, J. Alloy. Compd. 329 (2001) 142–152.
[68] Z. Zou, M. Simonelli, J. Katrib, G. Dimitrakis, R. Hague, Microstructure and tensile properties of additive manufactured Ti-6Al-4V with refined prior-β grain structure obtained by rapid heat treatment, Mater. Sci. Eng.: A 814 (2021) 141271.